Journal of Luminescence 132 (2012) 1015–1020

Contents lists available at SciVerse ScienceDirect

Journal of Luminescence

journal homepage: www.elsevier.com/locate/jlumin

Spectroscopy study of $SrAl_2O_4:Eu^{3+}$

Bento F. dos Santos Jr.*, Marcos V. dos Santos Rezende, Paulo J.R. Montes, Romel M. Araujo, Marcos A.C. dos Santos, Mário E.G. Valerio

Physics Department, Federal University of Sergipe, Campus Universitário, 491000-000 São Cristovão-SE, Brazil

ARTICLE INFO

Article history:
Received 29 April 2011
Received in revised form
27 August 2011
Accepted 2 September 2011
Available online 14 September 2011

Keywords:
Computer modeling
Intensity parameters
Simple overlap model

ABSTRACT

Computational and experimental method is employed to study optical properties $SrAl_2O_4$ induced by europium dopant. Atomistic modeling is used to predict the doping sites and charge-compensation schemes for $SrAl_2O_4$:Eu systems and also to calculate the symmetry and the detailed geometry of the dopant site. This information is then used to calculate the crystal field parameters. $SrAl_2O_4$ doped with europium were prepared via a sol–gel proteic methodology. The photoluminescence experiments were performed at room temperature and at 13 K. The transition energy for the Eu^{3+}-doped material is compared to the theoretical results. Based on Judd-Ofelt approach, the intensity parameters $\Omega_{2,4}$ of Eu^{3+} in the $SrAl_2O_4$ matrix were calculated.

1. Introduction

Strontium aluminates have attracted intense research, since they have interesting optical properties, of which the long last-phosphorescence is one of the most studied one due to technologic application [1]. This property is observed when the strontium aluminates are doped and double-doped with rare earth ions. Strontium aluminates have different crystallographic structures depending on the $SrO:Al_2O_3$ ratio. Most of them exhibit long last-phosphorescent when doped with rare earth, for example: $Sr_4Al_{14}O_{25}:Eu^{2+}$, Dy^{3+}, B^{3+} [2], $SrAl_4O_7:Eu^{2+}$, Dy^{3+} [3], $SrAl_{12}O_{19}$: Eu^{2+}, $Sr_2Al_6O_{11}:Eu^{2+}$ [4]. The $SrAl_2O_4:Eu^{2+}$, Dy^{3+}, B^{3+} [5,6] is the system that is reported in the literature as having the longest and the most efficient phosphorescence.

$SrAl_2O_4$ is observed in two different crystallographic forms with a reversible phase transition at 650 °C [7]. At room temperature the monoclinic phase is observed, while at high temperature the hexagonal phase is predominant. There are four different strontium sites (Sr1, Sr2, Sr3 and Sr4) and four different aluminum (Al1, Al2, Al3 and Al4) with tetrahedral coordinated in the monoclinic phase. The luminescent properties of trivalent rare earth doped $SrAl_2O_4$ are absent in the hexagonal phase.

Divalent rare earth doping is also reported in the literature. Eu^{2+} ions were found to generate luminescent center in the green region of the visible spectra, with $\lambda_{max}=520$ nm in the $SrAl_2O_4$ matrix [14]. When samples were produced by the sol–gel method and co-doped with Dy^{3+} in the $SrAl_2O_4$:Eu, Dy system, the main emission shifts to 500 nm when excited at 304 nm or 321 nm [15].

The proteic sol–gel process uses coconut water as the starting solvent [8]. A number of previous papers showed that this methodology can be successfully used to produce Y_2O_3 [9,10], $SrFe_{12}O_{19}$ [11], $BaFe_{12}O_{19}$ [12] and ZnO [13]. The organic molecules present in the coconut water (mainly proteins and lipids) can form a gel where the metallic ions can be anchored during the calcination step, the organic part is burnt and the oxides are formed.

The paper was divided in two parts. In the first one, a hybrid computer modeling method was employed, using a combination of defect calculations, based on lattice energy minimization and crystal field calculations. The output of this part is the defect type that is energetically favoured and the set of crystal field parameters, B_q^k, which are then used to calculate the energies of the 4f–4f electronic transitions of the europium trivalent ions. In the second part, samples of $SrAl_2O_4$ doped with europium were prepared via a sol–gel proteic methodology. Photoluminescence emission and excitation spectra of $SrAl_2O_4:Eu^{3+}$ were measured at room temperature and 13 K. The combination of the experimental and modeling techniques was useful to reveal some of the important features of the light emission processes in this material.

2. Methodology

2.1. Computer modeling

The computer modeling was divided in three different and complementary techniques. In the first one, the methodology uses

---

* Corresponding author. Tel.: +55 79 3248 5054.
E-mail address: bentofsjster@gmail.com (B.F. dos Santos Jr.).

0022-2313/$ - see front matter © 2011 Elsevier B.V. All rights reserved.
doi:10.1016/j.jlumin.2011.09.008

lattice minimization energy, where the interactions between the ions present on the material are parameterized via an interatomic Buckingham potential. The potentials to describe the system were obtained via an empirical approach embodied in the GULP code [16] where the potential parameters were fitted to the structures of all known strontium aluminate crystalline phases. The potentials were obtained in a previous paper [17]. The potentials for the europium ion–oxygen interactions were obtained from Araujo et al. [18]. Defect energies and final relaxed configuration were performed using the Mott-Littleton method [19] in which atoms in a spherical region immediately surrounding the defect are treated explicitly, and a continuum approach is used for more distant regions of the lattice. In the second step, the relaxed positions of the dopant and the surrounding ions are then input into a crystal field calculation based on the simple overlap model (SOM) [20] giving the crystal field parameters, B_q^k, as well as the intensity parameters Ω_2 (cm^{-1}) and Ω_4 (cm^{-1}). The latter are obtained using the equation:

$$\Omega_\lambda = (2\lambda+1)\sum_{t,p}\frac{\left|B_{\lambda,t,p}\right|^2}{(2t+1)} \tag{1a}$$

with

$$B_{\lambda,t,p} = B^{ac}_{\lambda,t,p} + B^{de}_{\lambda,t,p} \tag{1b}$$

where $\lambda = 2, 4$ and $t = 1, 3, 5, 7$ and $p = 0, \pm 4$ (the allowed values of p depend on the symmetry around the rare earth ion) are the intensity parameters coefficient, Ω_λ and $B_{\lambda tp}$ are the contributions of the forced electric dipole mechanism $B^{de}_{\lambda,t,p}$ and of the dynamic acoplament mechanism $B^{ac}_{\lambda,t,p}$.

In the third step, the B_q^k's were used to calculate the energies of the 4f–4f electronic transitions via the modified crystal field theory based on the Judd-Ofelt theory [21,22]. In this theory, the interaction between the rare-earth ion and the surrounding (host crystal) ions is given by the Hamiltonian $H_{\mathbf{CF}}$ that is basically dependent on the first coordination shell of the Eu^{3+} ions. This same methodology was already been successfully employed in a previous work [23].

2.2. Experimental part

The samples of $SrAl_2O_4$ and $Sr_{0.97}Eu_{0.03}Al_2O_4$ were produced via a new sol–gel route [8]. Solutions of $Sr(NO_3)_2$, $Al(NO_3)_3 \cdot 9\,H_2O$ and $EuCl_3 \cdot 6\,H_2O$ were mixed with natural coconut water (*Cocos nucifera*) forming the starting gels. The gel was dried at 100 °C for 24 h forming a xerogel. The xerogel was calcined following a heating program with a heating rate of 5 °C/min up to 1100 °C and kept at this temperature for a duration of 4 h [24]. The crystalline phases were identified by powder X-ray diffraction measurements using CuKα radiation with a Rigaku Ultima+ RINT 2000/PC diffractometer in the Bragg–Brentano geometry, operating at 40 kV/40 mA. All measurements were performed within the 2θ range from 10 to 80° at a scan speed of 2 °/min. The photoluminescence (PL) spectroscopy measurements were carried out using an ISS PC1 spectrofluorimeter at room temperature and at 13 K.

The phenomenological intensity parameters are obtained from the emission spectra of Eu doped $SrAl_2O_4$. The emission intensity, I, of a given transition is proportional to the area, S, under the emission curve

$$I = \hbar\omega_{0\to J}A_{0\to J}N \propto S \tag{2}$$

where $\hbar\omega_{0\to J}$ is the transition energy, N is the population of the emission level ($^5D_0$) and $A_{0\to J}$ is the spontaneous emission coefficient that can be calculated using the $^5D_0\to{}^7F_1$ transition as a reference. Thus $A_{0\to J}$ values can be evaluated using the expression:

$$A_{0\to J} = \frac{\sigma_{0\to 1}}{\sigma_{0\to J}}\frac{S_{0\to J}}{S_{0\to 1}}A_{0\to 1} \tag{3}$$

where $S_{0\to J}$ is the area under the $^5D_0\to{}^7F_J$ emission and $\sigma_{0\to J}$ is the transition barycenter.

The $^5D_0\to{}^7F_J$ transition is used as reference, because it is allowed transition via magnetic dipole mechanism, thus making $A_{0\to J}$ quite independent on the crystal field. $A_{0\to 1}$ can be related to the transition barycenter and the refraction index n via:

$$A_{0\to 1} = 0.31 \times 10^{-11}n^3(\sigma_{0\to 1})^3 \tag{4}$$

The phenomenological intensity parameters Ω_2 and Ω_4 are obtained from emission spectra of Eu^{3+} using the following expressions:

$$\Omega_2 = \frac{A_{0\to 2}}{2.33 \times 10^8(\sigma_{0\to 2})^3((n(n^2+2)^2)/9)} \tag{5}$$

and

$$\Omega_4 = \frac{A_{0\to 4}}{2.40 \times 10^8(\sigma_{0\to 4})^3((n(n^2+2)^2)/9)} \tag{6}$$

where $\frac{n(n^2+2)^2}{9}$ is the Lorentz factor.

3. Results and discussion

Formation energy for europium doping in $SrAl_2O_4$ matrix is shown in Table 1. The notation used for the different symmetries is explained in the appendix. Kroger–Vink notation [25] is employed to identify the defects. The temperature effect was included in the modeling considering just the harmonic approximation. The $SrAl_2O_4$ in the monoclinic phase were simulated at 0 K and at room temperature.

The formation energy is defined by the energy difference between the defective lattice, where one single defect is created, and the perfect lattice. This quantity cannot be used for comparison purposes, because the formation energy only involves the creation of a defect in the lattice. Thus, the solution energy is calculated, which includes all the terms in the thermodynamic cycle involved when the solution process occurs, including charge compensation mechanisms if needed. The solution energies were based on solid state reactions involved in the doping process of the material. In $SrAl_2O_4$ lattice there are two possibilities for the location of the dopant ions and several possibilities for charge compensation. Substitution might occur at either the Sr or Al site. Five different schemes were considered in this work and they are summarized in Table 2, with their related solid state reactions. For each one of the schemes more than one non-equivalent arrangement of the basic defects is possible, and they are explained in detail in the Appendix.

From the solution energy values presented in Table 1 it can be seen that incorporation of europium is likely to occur at the strontium site at both temperature. The lowest-energy charge compensation mechanism involves substitution at the Sr site with oxygen interstitial compensation. Since two Eu^{3+} are needed for each oxygen interstitial, more than one configuration is possible and several non-equivalent configurations were analyzed, as quoted in Table 1. The solution energies obtained at 300 K for the D5 configuration is the lowest one and that corresponds to Eu ions substituting at two different Sr sites, Sr1 and Sr3 (see Appendix). At 0 K, on the other hand, the D4 configuration is the one with lowest solution energy and that involves Eu^{3+} ions at Sr3 and Sr4 sites.

The solution energy for incorporation of europium at Al site is higher comparing with the incorporation at Sr site. The dopant

Table 1
Formation energy and solution energy for europium ion in the $SrAl_2O_4$ lattice at 0 K and 300 K.

Eu									
	Formation energy		Solution energy (eV)			Formation energy		Solution energy (eV)	
Defects	0 K	300 K	0 K	300 K	Defects	0 K	300 K	0 K	300 K
M_{Al}					$2M_{Sr}$–O_i				
Al1	15.09	14.93	2.26	2.24	D1	−57.94	−58.79	1.93	1.61
Al2	15.13	14.97	2.30	2.28	D2	−58.98	−59.83	1.58	1.27
Al3	15.15	14.99	2.32	2.30	D3	−58.77	−59.01	1.65	1.54
Al4	15.19	15.02	2.36	2.33	D4	−60.06	−59.48	1.22	1.38
$2M_{Sr}$–V_{Sr}					D5	−59.74	−60.38	1.33	1.08
B1	−23.52	−24.25	1.92	1.66	D6	−59.11	−60.31	1.54	1.11
B2	−23.98	−24.67	1.77	1.52	$3M_{Sr}$–V_{Al}				
B3	−24.26	−24.92	1.68	1.43	E1	−9.84	−10.53	1.66	1.50
M_{Sr}–Sr_{Al}					E2	−8.99	−9.71	1.87	1.70
C1	15.84	15.06	1.51	1.19	E3	−9.87	−10.42	1.65	1.53
C2	16.21	15.45	1.69	1.38	E4	−8.31	−9.30	2.04	1.81
C3	15.81	15.03	1.49	1.17	E5	−9.75	−10.63	1.68	1.48
C4	15.88	15.10	1.53	1.21	E6	−7.64	−8.30	2.21	2.06
C5	16.32	15.53	1.75	1.42	E7	−9.98	−10.71	1.62	1.46
C6	16.10	15.29	1.64	1.30	E8	−9.86	−10.53	1.65	1.50
C7	15.70	14.92	1.44	1.12	E9	−9.11	−9.83	1.84	1.67
C8	15.80	14.99	1.49	1.15					

Table 2
Solid state reactions associated to the different schemes for incorporation of europium ion in the $SrAl_2O_4$ lattice.

All possible configurations	Reaction schemes
(i) Substitution at the Al^{3+} site (no charge compensation needed)	$\frac{1}{2}Eu_2O_3+Al_{Al}\rightarrow Eu_{Al}+\frac{1}{2}Al_2O_3$
(ii) Substitution at the Sr^{2+} site (charge compensation by Sr^{2+} vacancies)	$Eu_2O_3+3Sr_{Sr}\rightarrow(2Eu^{\cdot}_{Sr}-V''_{Sr})+3SrO$
(iii) Substitution at the Sr^{2+} site (charge compensation by Sr^{2+}/Al^{3+} substitution)	$\frac{1}{2}Eu_2O_3+Sr_{Sr}+Al_{Al}\rightarrow(Eu^{\cdot}_{Sr}+Sr'_{Al})+\frac{1}{2}Al_2O_3$
(iv) Substitution at the Sr^{2+} site (charge compensation by O^{2-} interstitial)	$Eu_2O_3+2Sr_{Sr}\rightarrow(2Eu^{\cdot}_{Sr}-O''_i)+2SrO$
(v) Substitution at the Sr^{2+} site (charge compensation by Al^{3+} vacancies)	$\frac{3}{2}Eu_2O_3+3Sr_{Sr}+Al_{Al}\rightarrow(3Eu^{\cdot}_{Sr}-V'''_{Al})+3SrO+\frac{1}{2}Al_2O_3$

Table 3
The crystal fields parameters for two strontium sites.

B^k_q	Eu3 site	Eu4 site
B^2_0	769	774
B^2_1	556	−988
B^2_2	50	981
B^4_0	184	−351
B^4_1	83	−485
B^4_2	47	389
B^4_3	126	−532
B^4_4	32	−103
B^6_0	−196	85
B^6_1	−88	384
B^6_2	−38	−314
B^6_3	197	−93
B^6_4	152	294
B^6_5	51	−539
B^6_6	16	−95

and Al ions have the same oxidation number, but the distortion caused by the large different between ionic radii between the dopant ion and the aluminum ions (0.947 and 0.39 Å [26], respectively) are quite large increasing the energy cost to accommodate the Eu^{3+} at Al lattice site.

From the atomistic calculations, relaxed positions of the europium ions and the surrounding lattice ions are obtained. This information is then used to calculate the crystal field parameters, B^k_q, which are given in Table 3. The crystal field parameters were calculated for the incorporation of the europium in both strontium sites (Sr1 and Sr3), which is due to a great possibility of europium incorporation in both the sites, confirmed for the solution energy given in Table 1. From Table 4, it is noted that all parameters are non-zero in both sites, indicating that the symmetry of the substitution site is low and that the deformation caused for incorporation of europium in the lattice is large. This is due a little space in the strontium site in $SrAl_2O_4$ compared with other strontium aluminates Fig. 1.

The XRD patterns of $SrAl_2O_4$ powders obtained at 1100 °C/4 h are shown in Fig. 2. The comparison of the experimental XRD pattern with the standard pattern [7] indicates that single phase crystallites were obtained.

Fig. 2 shows the emission spectra of the $SrAl_2O_4:Eu^{3+}$ sample calcined at 1100 °C for 4 h excited at 265 nm at room temperature and at 13 K. Typical emission peaks of Eu^{3+} can be observed in the range of 13000–18000 cm^{-1} and assigned to the transitions from $^5D_0$ to ^7F_J ($J=0, 1, 2, 3, 4$).

There are two peaks at about 17352.2 and 17392.1 cm^{-1} that are due to the $^5D_0\rightarrow{}^7F_0$ transition, indicating that Eu ion can be substituted into the two non-equivalent sites. This result agrees well with the prediction obtained from computer simulation that the Eu ion can be substituted into two different Sr sites for both temperatures.

It is also noticeable that among all emission peaks, the one at 16226.0 cm^{-1} due to the electric dipole transition of $^5D_0\rightarrow{}^7F_2$ is the strongest. It is well known that this Eu^{3+} ion is especially sensitive and it is strongly influenced by the surrounding environment [27]. When Eu^{3+} ions occupy the sites with higher symmetry, the emission from the $^5D_0\rightarrow{}^7F_2$ transition is usually very weak; otherwise, the emission will be strong [28]. The existence of this dominant emission shows that the Eu^{3+} sites

Table 4
Comparison of the predicted and experimental energy transition of Eu^{3+} in the $SrAl_2O_6$ matrix at low temperature. Assuming substitution at both strontium sites.

Transition	Eu1 site Energy theo. (cm^{-1})	Eu3 site Energy theo. (cm^{-1})	Eu1 site Energy exp. (cm^{-1})	Eu3 site Energy exp. (cm^{-1})
$^5D_0 \rightarrow {}^7F_0$	17808.2	17832.4	17352.2 (1)	17392.1 (1)
$^5D_0 \rightarrow {}^7F_1$	17576.3	17697.6	17218.1 (1)	17141.0 (10)
	17470.5	17457.7	16971.4 (7)	16946.9 (5)
	17127.4	16907.9	16935.6 (1)	16918.9 (9)
$^5D_0 \rightarrow {}^7F_2$	16864.9	16680.2	16204.8 (200)	15943.7 (5)
	16859.0	16742.4	16307.1 (3)	15868.6 (2)
	16631.5	16432.2	16168.3 (5)	15811.1 (5)
	16609.7	16418.8	16135.0 (2)	15635.2 (2)
	16487.8	16248.7	15993.4 (4)	15594.5 (1)
$^5D_0 \rightarrow {}^7F_3$			15148.8 (6)	
	15939.2	15995.7	15396 (118)	
	15938.4	15942.6	15422.2 (50)	
	15929.4	15735.1	15339.2 (2)	
	15845.8	15653.9	15311.8 (1)	
	15842.9	15559.2	15222.9 (2)	
	15749.2	15549.0	15189.4 (1)	
	15722.4	15431.3	14423.4 (2)	
$^5D_0 \rightarrow {}^7F_4$			15371.4 (122)	
	14908.5	14880.8	14526.9 (7)	
	14903.1	14844.6	14484.7 (3)	
	14891.6	14795.0	14365.9 (1)	
	14823.4	14714.5	14337.7 (10)	
	14820.1	14624.4	14232.3 (7)	
	14817.5	14595.6	14199.2 (2)	
	14805.3	14551.2	14065.6 (5)	
	14778.9	14536.1	14002.1 (30)	
	14776.0	14471.2	13913.5 (6)	

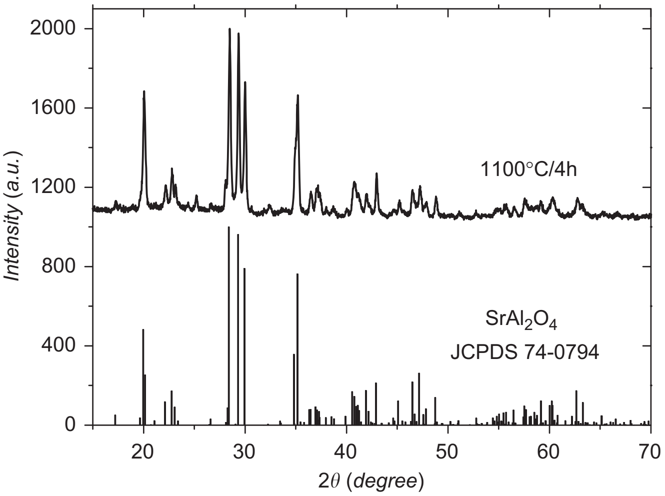

Fig. 1. Diffractogram of $SrAl_2O_4$:Eu.

have low symmetry. This result agrees well with the predictions obtained from computer simulation that the dopant occupies the strontium sites, that is already a low symmetry site, but is even further lower due to the interstitial O^{2-} ion nearby. This result is also supported after calculating the B_q^k parameters and showing that all of them are non-zero, for all Eu^{3+} sites. Electron paramagnetic resonance (EPR) study on $SrAl_2O_4$:Eu^{2+} by Kaiya et al. [29] found that the Eu ions occupy the strontium sites with lower symmetry, which is consistent with the theoretical and experimental results presented wherein.

Emission spectra measurements taken at 300 K , shown in the Fig. 2, exhibits the following peaks associated to the following transitions: one peak due to $^5D_2 \rightarrow {}^7F_2$ at 20576.1 cm^{-1}, one peak due to $^5D_2 \rightarrow {}^7F_3$ in 19685.0 cm^{-1}, one peak at 17730.5 cm^{-1} due to the $^5D_0 \rightarrow {}^7F_0$ transition, three peaks around 17513.1, 17452.0 and 16920.5 cm^{-1} related to the $^5D_0 \rightarrow {}^7F_1$ transitions, four peaks corresponding to the $^5D_0 \rightarrow {}^7F_2$ transition, two peaks to the corresponding to the $^5D_0 \rightarrow {}^7F_3$ transition and five peaks corresponding to the $^5D_0 \rightarrow {}^7F_4$ transitions.

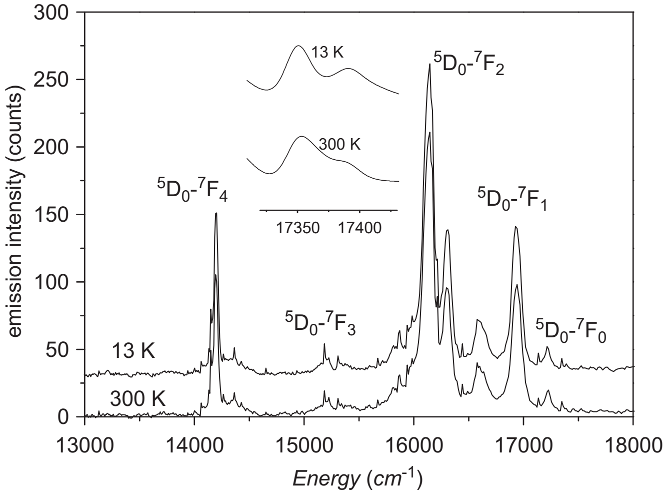

Fig. 2. Spectrum of the emission of $SrAl_2O_4$:Eu (excited at 265 nm) at 300 K and 13 K.

The room temperature measurements are not ideal to identify all transitions related to the Eu^{3+} ions in the $SrAl_2O_4$ matrix. This problem can been resolved measuring the emission spectra at low temperature. In Fig. 2, the emission spectra obtained at 13 K and 300 K are also shown.

The inset in Fig. 2 shows the region between 17320 and 17450 cm^{-1}, where it can be seen that there are two peaks due to the $^5D_0 \rightarrow {}^7F_0$ transition. This observation is in agreement with the modeling prediction that the Eu^{3+} should be in 2 different sites.

The asymmetric ratio *R* is defined as the ratio of the intensity of the $^5D_0 \rightarrow {}^7F_1$ to the $^5D_0 \rightarrow {}^7F_2$ transitions. The higher the *R* value the stronger the covalence of Eu^{3+}–O^{2-} ions and the lower the site symmetry [30]. In $SrAl_2O_4$:Eu^{3+}, the *R* value is about 2.1 indicating that Eu^{3+} site-symmetry is lower and the chemical bonds have a quite high degree of covalence. In the case of lanthanides, as the interaction between the central ion and its ligating ions is essentially ionic, the low symmetry should play the dominant role for this system.

In Table 4 the difference between the predicted and the experimental energy transition of Eu^{3+} in the $SrAl_2O_4$ lattice are shown. The theoretical transition energies were obtained for Eu^{3+} ions at both Sr1 and Sr3 for 0 K. The experimental transition energies were obtained after fitting the experimental curves to Gaussian shape profiles. Comparing the theoretical and experimental values for the $^5D_0 \rightarrow {}^7F_0$ transition, it can be seeing that the peak at 17352 cm^{-1}, that correspond to the stronger $^5D_0 \rightarrow {}^7F_0$ transition is due to the Eu^{3+} ions substituting at the Sr1 site, while the weaker $^5D_0 \rightarrow {}^7F_0$ transition related to the peak at 17392.0 cm^{-1} is due to the Eu^{3+} ions at Sr3 site. The average difference between the predicted and the experimental values of the energies for the $^5D_0 \rightarrow {}^7F_0$ and $^5D_0 \rightarrow {}^7F_1$ transitions is around ~3%.

The $^5D_0 \rightarrow {}^7F_1$ transitions is composed by three lines for each Eu^{3+} site and in the emission spectra it was possible to identify all of then connected to the 2 different sites of Eu^{3+}. That can be done simply by comparison between the experimental and the predicted values for each one of the transitions. The experimental splitting of the $^5D_0 \rightarrow {}^7F_1$ transitions is about 250 cm^{-1}, while the predicted value is ~ 450 cm^{-1} for Eu^{3+} at the Sr1 site and ~ 750 cm^{-1} for the Eu^{3+} at the Sr3 site. The splitting predicted for $^5D_0 \rightarrow ^7F_2$ transitions is about 400 cm^{-1} for both Eu sites and the experimental value is $\sim$ 200 cm^{-1} for the Eu at the Sr1 site and $\sim$ 350 cm^{-1} for the Eu^{3+} at the Sr3 site.

The situation of the $^5D_0 \rightarrow ^7F_j$ ($j=3,4$) transitions is not so clear and it is not possible to find all lines associated to the transitions for each one of the Eu^{3+} sites. This is due to the superposition of a great number of emission lines in a small range of the spectra. As an example, when Eu^{3+} is at the Sr3 site, one should expect 7 lines associated to the $^5D_0 \rightarrow ^7F_3$ transition in the wave number interval of $\sim$600 cm^{-1}, between 15431.3 and 15995.7 cm^{-1}. Taking into account that the Eu^{3+} is located at 2 different sites, that would make 14 lines within roughly the same range. It means that the splitting would be only experimentally accessible with very high resolution spectrometer, that is not the case here. Similar effect happens for the $^5D_0 \rightarrow ^7F_4$ transitions with the exception that one should now expect 9 lines for each of the Eu^{3+} sites, making a total of 18 lines in the range from 14400 to 14900 cm^{-1}. In Table 5, measured energies for these transitions were grouped as one single group but the predicted values are separated according to their sites. It is possible to observe that, despite the fact it was not possible to separate the sites; the experimental wave numbers are in a reasonable good agreement with the predicted values.

The coordinates of the ligand oxygen were taken from the strontium aluminate data and the Eu–O distances have been used to calculate the effective's charges (g) and their polarizabilities showed in Tables 5 and 6, for the Eu1 and Eu3 sites, respectively. The integrated areas of the emission spectrum (Fig. 2) have been used to calculate the intensity parameters, which allow a prediction of the emission characteristics of the RE^{3+} ion in a particular host [40]. Using Eqs. (3)–(6), the experimental or phenomenological intensity parameters Ω_2 and Ω_4 could be evaluated. The Ω_6 intensity parameter was not included in this study since the $^5D_0 \rightarrow ^7F_6$ transition could not be observed and this transition presents, in general, an extremely low intensity [41]. In addition, Ω_2 and Ω_4 were also calculated using the modeling approach described wherein via Eq. (1) and the crystal field parameters obtained for each one of the Eu^{3+} sites in the matrix. This is the first time that the absolute values of the intensity parameters (Ω_2, Ω_4) are reported for aluminate crystals. These values are quoted in Table 7 with other values of Ω_2 and Ω_4 found in the literature.

Table 5
Ligand coordinates for site one (R in units of 10^{-8} cm and angles of $\pi/180$) and their polarizability (α in units of 10^{-24} cm^3).

R	θ	φ	α	g
2.3475	40.5521	−5.3837	3.13	0.22997
2.6311	130.4116	5.5427+180	4.28	0.28267
2.5509	71.6374	40.6431+180	4.28	0.28267
2.3880	146.3510	82.2428	3.13	0.22997
2.2286	64.9108	−62.8027+180	5.50	0.98736
2.5142	104.1068	−84.7505	5.40	0.98736

Table 6
Ligand coordinates for site two (R in units of 10^{-8} cm and angles of $\pi/180$) and their polarizability (α in units of 10^{-24} cm^3).

R	θ	φ	α	g
2.3080	70.6642	−6.8653	1.82	0.22997
2.4349	156.0441	5.5427+180	4.30	0.28267
2.7742	48.4661	40.6431+180	4.30	0.28267
2.3488	115.1548	78.5199	1.82	0.22997
2.5178	49.5681	−65.0518+180	6.17	0.98736
2.3488	113.5996	−98.5199	6.17	0.98736

Table 7
Intensity parameters of $SrAl_2O_4:Eu^{3+}$ and other selected matrixes.

Matrix	Ω_2 (10^{-20} cm^2)	Ω_4 (10^{-20} cm^2)	Refs.
Fluoride glasses	0.51	4.19	[31]
$LaF_3:Eu^{3+}$ crystal	1.19	1.16	[32]
$Sr(PO_3)_2$ glasses	5.90	1.4	[33]
Phosphate glasses	6.91	5.01	[34]
Silicate glasses	9.65	5.58	[35]
$Y_2O_3:Eu^{3+}$	9.90	3.60	[36]
$Y_2O_3:Eu^{3+}$,Co	11.06	–	[37]
$SrAl_2O_4:Eu^{3+}$ (Exp.)	26.592	5.7548	Present work
$SrAl_2O_4:Eu^{3+}$ (SOM) site 1	26.400	5.7411	Present work
$SrAl_2O_4:Eu^{3+}$ (SOM) site 2	29.204	5.7735	Present work

Judd-Ofelt intensity parameters reflect local structure and bonding in the vicinity of Eu ions. For example, Ω_2 exhibits the dependence on the covalence between Eu ions and ligand anions and gives information about the asymmetry of the local environment of Eu^{3+} site [38]. The three intensity parameters Ω_2, Ω_4 and Ω_6 may be regarded as phenomenological parameters characterizing the radiation transition probabilities within the ground configuration [39].

The theoretical intensity parameters obtained by SOM and electrostatic equilibrium theory [20,42] and the characteristic emission spectra of Eu in this compound shows high value of the Ω_2 intensity parameters, reflecting the hypersensitive behavior of the $^5D_0 \rightarrow ^7F_2$ transition and indicating that the rare earth ion is in a highly polarizable chemical environment. This result suggests that the short distance effects are dominant. The Ω_2 in $SrAl_2O_4$ is larger than those of other materials quoted in Table 7. The Ω_4 values for $SrAl_2O_4$:Eu system, on the other hand, have roughly the same values as the other materials, excepted for the LaF_3 matrix and the $Sr(PO_3)_2$ glass.

An interesting result is that the experimental intensity parameters obtained from the emission spectra agreed quite well with the values obtained in the modeling part, with a difference around 1% and 0.3% for Ω_2 and Ω_4 , respectively.

4. Conclusion

The proteic sol–gel route was found to be a reliable method for the synthesis of europium doped $SrAl_2O_4$. XRD analysis shows that the desired crystalline phase was obtained. Emission spectrum indicates the presence of Eu^{3+} in the samples. The results indicate that europium ion preferentially substitutes at both the Sr sites with oxygen interstitial compensation charge defect. The crystal field parameters, B_q^k, and the transition energies were calculated for each Eu^{3+} site and the predicted values agreed quite well with the experimental values, with a difference around 3%. Judd-Ofelt intensity parameters Ω_2 and Ω_4 have been derived from the emission spectrum and from the theoretical modeling based on the Electrostatic equilibrium theory and the agreement between the experimental and the predicted values are very good. It is the first time that the intensity parameters Ω_2 and Ω_4 are reported in the literature for the case of $SrAl_2O_4$:Eu systems. As an overall conclusion, the combination of different modeling techniques with experimental results revealed interesting aspects of the optical activity of Eu^{3+} ions in the $SrAl_2O_4$ matrix that could not be accessible as separate works. The same strategy can be applied to a number of other systems where samples were readily available.

Acknowledgments

The authors are grateful to INCT-INAMI, FAPIEC/SE, CNPq. CAPES and FINEP for financial support.

Table A1
Formation energy of different symmetries of the defect at 0 K and 293 K.

Configurations					
A1	Al1	C4	$\mathrm{M_{Sr2}{-}Sr2_{Al4}}$	D6	$\mathrm{M_{Sr1}{-}M_{Sr3}{-}O2_{i}}$
A2	Al2	C5	$\mathrm{M_{Sr3}{-}Sr2_{Al1}}$	E1	$\mathrm{M_{Sr1}{-}M_{Sr2}{-}M_{Sr3}{-}V_{Al1}}$
A3	Al3	C6	$\mathrm{M_{Sr3}{-}Sr2_{Al2}}$	E2	$\mathrm{M_{Sr1}{-}M_{Sr2}{-}M_{Sr3}{-}V_{Al2}}$
A4	Al4	C7	$\mathrm{M_{Sr3}{-}Sr2_{Al3}}$	E3	$\mathrm{M_{Sr1}{-}M_{Sr2}{-}M_{Sr3}{-}V_{Al3}}$
B1	$\mathrm{M_{Sr1}{-}M_{Sr3}{-}V_{Sr4}}$	C8	$\mathrm{M_{Sr3}{-}Sr2_{Al4}}$	E4	$\mathrm{M_{Sr1}{-}M_{Sr2}{-}M_{Sr3}{-}V_{Al4}}$
B2	$\mathrm{M_{Sr1}{-}M_{Sr3}{-}V_{Sr4}}$	D1	$\mathrm{M_{Sr1}{-}M_{Sr3}{-}O1_{i}}$	E5	$\mathrm{M_{Sr2}{-}M_{Sr3}{-}M_{Sr4}{-}V_{Al1}}$
B3	$\mathrm{M_{Sr2}{-}M_{Sr4}{-}V_{Sr3}}$	D2	$\mathrm{M_{Sr1}{-}M_{Sr2}{-}O2_{i}}$	E6	$\mathrm{M_{Sr1}{-}M_{Sr3}{-}M_{Sr4}{-}V_{Al1}}$
C1	$\mathrm{M_{Sr2}{-}Sr2_{Al1}}$	D3	$\mathrm{M_{Sr1}{-}M_{Sr3}{-}O2_{i}}$	E7	$\mathrm{M_{Sr1}{-}M_{Sr3}{-}M_{Sr4}{-}V_{Al2}}$
C2	$\mathrm{M_{Sr2}{-}Sr2_{Al2}}$	D4	$\mathrm{M_{Sr3}{-}M_{Sr4}{-}O2_{i}}$	E8	$\mathrm{M_{Sr1}{-}M_{Sr3}{-}M_{Sr4}{-}V_{Al3}}$
C3	$\mathrm{M_{Sr2}{-}Sr2_{Al3}}$	D5	$\mathrm{M_{Sr1}{-}M_{Sr4}{-}O2_{i}}$	E9	$\mathrm{M_{Sr1}{-}M_{Sr3}{-}M_{Sr4}{-}V_{Al4}}$

Appendix A. Explanation of symmetry notation used in Table 1

In this appendix all the formation and solution energies calculated for the mechanism of incorporation of trivalent rare earth dopants in $SrAl_2O_4$ are presented. The explanation of symmetry notation used in tables below is also given.

On doping the $SrAl_2O_4$ in the the monoclinic P21 phase two issues should be considered: (i) there are 4 Al and 4 Sr sites where the dopant could be present; and (ii) the doping mechanism involving charge compensating defects will have more than one non-equivalent ways of arranging the basic defects in the lattice giving rise to different configurations of the full defect. These two aspects were taken into account on computing the formation and the solution energies.

Table A1 displays the symmetry notation used in all following tables. The first four defects, A1 to A4, are just the trivalent dopants in one of the four Al sites. This is the only type of defect that does not need charge compensation accompanying defects. Defects B1 to B3 are the possible ways of arranging two trivalent dopants in the two Sr sites accompanied by one Sr vacancy as charge compensation. Defects C1 to C8 are all the possibilities to have the dopant in one of the Sr sites plus a Sr at any one of the four Al sites. As an example, defect B1 is formed by 2 trivalent dopants at Sr1 and Sr2 sites compensated by a vacancy of Sr4 site. The other defects just follow the same general idea.

References

[1] F. Clabau, X. Rocquefelte, S. Jobic, S. Deniard, M.-H. Whangbo, A. Garcia, T.L. Mercier, Chem. Mater. 17 (2005) 3904.
[2] Y. Lin, Z. Tang, Z. Zhang, Mater. Lett. 51 (2001) 14.
[3] C. Chang, D. Mao, J. Shen, C. Feng, J. Alloys Compd. 348 (2003) 224.
[4] R. Zhong, J. Zhang, X. Zhang, S. Lu, X.-J. Wang, J. Lumin. 119 (2006) 327.
[5] Y. Murayama, N. Takeuchi, Y. Aoki, T. Matsuzawa, U.S. Patent No. 5,424,006, 1995.
[6] T. Peng, L. Huajun, H. Yang, C. Yan, Mater. Chem. Phys. 85 (2004) 68.
[7] A.R. Schulze, Hk. Mueller-Buschbaum, Zeitschrift fuer Anorganische und Allgemeine Chemie 475 (1981) 205–210.
[8] M.A. Macedo, J.M. Sasaki, Processo de Fabricação de Pós Nanoparticulados, INPI 0203876–5.
[9] P.J.R. Montes, M.A. Macedo, F.G.C. Cunha, Z.S. Macedo, M.E.G. Valerio, J. Metastable Nanocryst. Mater. 20 (2003) 247.
[10] P.J.R. Montes, M.E.G. Valerio, M.A. Macêdo, F. Cunha, J.M. Sasaki, Microelectron. J. 34 (2003) 557.
[11] P.C.A. Brito, R.F. Gomes, J.G.S. Duque, M.A. Macedo, Phys. B 384 (2006) 91.
[12] S.S. Fortes, J.G.S. Duque, M.A. Macedo, Phys. B 384 (2006) 88.
[13] N.O. Dantas, M.A.C. dos Santos, F. Cunha, M.A. Macedo, Phys. B 398 (2007) 291.
[14] T. Aitasalo, J. Hölsä, H. Jungner, J.-C. Krupa, M. Lastusaari, J. Legendziewicz, J. Niittykoski, Radiat. Meas. 38 (2004) 727.
[15] Z. Tang, F. Zhang, Z. Zhang, C. Huang, Y. Lin, J. Am. Ceram. Soc. 20 (2000) 2129.
[16] J.D. Gale, J. Chem. Soc. Faraday Trans. 93 (1997) 629.
[17] M.V. dos S. Rezende, R.M. Araújo, M.E.G. Valerio, R.A. Jackson, J. Phys.: Confe. Ser. 249 (2010) 012042.
[18] R.M. Araujo, K. Lengyel, R.A. Jackson, L. Kovács, M.EG. Valerio, J. Phys.: Condens. Matter 19 (2007) 046211.
[19] N.F. Mott, M.J. Littleton, Trans. Faraday Soc. 34 (1938) 485.
[20] O.L. Malta, Chem. Phys. Lett. 88 (1982) 353.
[21] B.R. Judd, Phys. Rev. 127 (1962) 750.
[22] G.S. Ofelt, J. Chem. Phys. 37 (1962) 511.
[23] M.V.S. Rezende, R.M. Araújo, P.J.R. Montes, M.G. Valerio, Opt. Mater. 32 (2010) 1341.
[24] P.J.R. Montes, M.E.G. Valerio, G.M. Azevedo, Nucl. Instrum. Methods Phys. Res., Sect. B 266 (2008) 2923.
[25] F.A. Kroger, H.J. Vink, J. Chem. Phys. 22 (1954) 250.
[26] R.D. Shannon, Acta Crystallogr. A 32 (1976) 751.
[27] M. Peng, J. Qiu, L. Yang, C. Zhao, Opt. Mater. 27 (2004) 591.
[28] M. Peng, N. Da, Y. Qiao, B. Wu, C. Wang, D. Chen, J. Qiu, J. Rare Earths 24 (2006) 749.
[29] K. Kaiya, N. Takahashi, T. Nakamura, T. Matsuzawa, G.M. Smith, P.C. Riedi, J. Lumin. 8789 (2000) 1073.
[30] G. Tang, J. Zhu, Y. Zhu, C. Bai, J. Alloys Compd. 453 (2008) 487.
[31] J. McDougall, D.B. Hollis, M.J.B. Payne, Phys. Chem. Glasses 35 (1994) 258.
[32] M.J. Weber, Optical Properties of Ions in Crystals, in: H.M. Crosswhite, H.W. Moos (Eds.), Wiley/Interscience Inc, New York, 1967, p. 467.
[33] S. Zaccaria, M. Casarin, A. Speghini, D. Ajó, M. Bettinell, Spectrochim. Acta Part A 55 (1999) 171.
[34] R. Balakrishnaiah, R. Vijaya, P. Babu, C.K. Jayasankar, M.L.P. Reddy, J. Non-Cryst. Solids 353 (2007) 1397.
[35] S.S. Babu, P. Babu, C.K. Jayasankar, W. Sievers, T. Troster, G. Wortmann, J. Lumin. 126 (2007) 109.
[36] Ž. Antic, R. Krsmanovic, V. Đor.evic, T. Dramicanin, M.D. Dramicanin, Acta Phys. Pol. A 116 (2009).
[37] A. Nayak, K. Goswami, A. Ghosh, R. Debnath, Indian J. Pure Appl. Phys. 47 (2009) 775.
[38] J. Wang, H. Song, X. Kong, H. Peng, B. Sun, B. Chen, J. Zhang, W. Xu, J. Appl. Phys. 93 (2003) 1483.
[39] G. Wang, W. Chen, Z. Li, Z. Hu, Phys. Rev. B 60 (1999) 15469.
[40] S.S. Babu, P. Babu, C.K. Jaysankar, W. Sievers, Th. Tröster, G. Wortmann, J. Lumin. 126 (2007) 109.
[41] O.L. Malta, Mol. Phys. 42 (1) (1981) 65.
[42] M.A. Couto dos Santos, Chem. Phys. Lett. 455 (2008) 339.